Karabanov, Alexander and Kwiatkowski, Grzegorz and Perotto, Carlo U. and Wiśniewski, Daniel and McMaster, Jonathan and Lesanovsky, Igor and Köckenberger, Walter (2016) Dynamic nuclear polarisation by thermal mixing: quantum theory and macroscopic simulations. Physical Chemistry Chemical Physics (46). pp. 30093-30104. ISSN 1463-9084

Journal Name

ARTICLE TYPE

Cite this: DOI: 10.1039/xxxxxxxxxx

Dynamic nuclear polarisation by thermal mixing: quantum theory and macroscopic simulations

Alexander Karabanov *[1], Grzegorz Kwiatkowski [1], Carlo Perotto [2], Daniel Wiśniewski [1], Jonathan McMaster [2], Igor Lesanovsky [1] and Walter Köckenberger [1]

Received Date
Accepted Date

DOI: 10.1039/xxxxxxxxxx

www.rsc.org/journalname

A theory of dynamic nuclear polarisation (DNP) by thermal mixing is suggested based on purely quantum considerations. A minimal 6-level microscopic model is developed to test the theory and link it to the well-known thermodynamic model. Optimal conditions for the nuclear polarization enhancement and effects of inhomogeneous broadening of the electron resonance are discussed. Macroscopic simulations of nuclear polarization spectra displaying good agreement with experiments, involving BDPA and trityl free radicals, are presented.

1 Introduction

Highly polarised nuclear spins have applications in many fields, from high-resolution spectroscopy and material science to particle physics and medical diagnostics (see, for example, [1–6]). Solid state DNP is a process of polarising a nuclear spin ensemble by an ensemble of unpaired electron spins irradiated by a microwave field at a certain frequency. Unlike the method of brute force where the nuclear system is transferred to a low temperature equilibrium [7], DNP is a dynamical process where the high nuclear polarisation is achieved by driving the electron-nuclear spin system far from its thermal equilibrium [8]. Due to electron-nuclear spin interactions, the high thermal polarisation of electrons is transferred to the nuclei resulting in a nuclear polarisation much higher than their thermal polarisation. In practice it is realised in single crystals or powder crystalline dielectrics doped with paramagnetic centres or diluted and then frozen samples doped with free radicals [5,6].

Three basic mechanisms are well-known to be responsible for DNP in solids [5], depending on the effective number of electron spins: solid effect (SE) [9], cross effect (CE) [10–12] and thermal mixing (TM) [13–15]. The SE involves single electron spins transferring their polarisation to nuclei via either zero- or double-quantum transitions. In the CE, a triple spin flip of two electrons and one nuclear spin transfers the polarization difference between the two electrons to the nuclear spin. TM is characterised by strong interactions between many electron spins making the electron spin ensemble act as a whole, transferring its uniform polarisation to nuclei via processes described in analogy to thermodynamic cooling. Recently, the importance of the direct electron-nuclear cross-relaxation, the Overhauser effect, as a basic mechanism for solid state DNP has also been experimentally and theoretically demonstrated [16].

Two basic approaches towards a theoretical description of DNP exist: microscopic quantum mechanical and macroscopic thermodynamic. In the quantum mechanical approach, dynamical ensembles are represented by sets of spins characterised by quantum operators with algebraic properties of an angular momentum. Spin interactions are represented by tensor products of individual spin operators and the dynamics behind DNP processes is represented in terms of the density operator obeying a master equation with given Hamiltonian and dissipative parts. The thermodynamic approach is based on the concept of spin temperature where different parts of the spin Hamiltonian are treated as heat reservoirs having thermal contacts with each other and exchanging their effective temperatures by thermodynamic rules leading to sets of linear rate equations describing the spin polarisation.

The SE and CE cases are currently well studied from both thermodynamic and quantum points of view. Minimal microscopic models have been developed and analysed. The difficulties caused by large dimensions of state spaces involved in the dynamics were overcome using averaging and projection techniques. Strong links to macroscopic simulations are established. The details of these aspects can be found in several works [17–23]. In the case of TM, the full qualitatively relevant and quantitatively applicable microscopic picture is missing. The TM DNP mechanism and its links to macroscopic experiments are currently discussed from a purely thermodynamic point of view.

The details of the thermodynamic model of TM DNP are well described and can be found in original works [13–15,24] and reviews [5,25,26] (some recent developments linking the spin temper-

* *Corresponding author: E-mail: karabanov@hotmail.co.uk; Tel: +44 (0) 115 8180011*

[1] *School of Physics and Astronomy, University of Nottingham, University Park, Nottingham, NG7 2RD, United Kingdom.*

[2] *School of Chemistry, University of Nottingham, University Park, Nottingham, NG7 2RD, United Kingdom*

ature concept applied to DNP with quantum mechanics can be found in[27–30]). According to the thermodynamic (spin temperature) model, the mechanism involves three energies: the electron Zeeman energy $H_S = \omega_S S_z$ (where ω_S is the electron frequency), the electron-electron coupling energy H_{SS} and the nuclear Zeeman energy $H_I = \omega_I I_z$ (where ω_I is the nuclear frequency). Each energy forms a heat reservoir with its own spin temperature, T_S, T_{SS} and T_I respectively, and the density operator of the system is represented by the joint Boltzmann distribution $\sigma \sim \exp(-\beta_S H_S - \beta_{SS} H_{SS} - \beta_I H_I)$ where the coefficients β are expressed via the corresponding temperatures as $\beta = \hbar/kT$ (so β are often called inverse temperatures). In the high-temperature limit $\sigma \sim 1 - \beta_S H_S - \beta_{SS} H_{SS} - \beta_I H_I$, the three energies generate the observables (polarisations) $\langle S_z \rangle$, $\langle H_{SS} \rangle$, $\langle I_z \rangle$ proportional to their inverse temperatures: $\langle S_z \rangle \equiv \mathrm{Tr}(\sigma S_z) \sim -\beta_S \omega_S \mathrm{Tr}(S_z^2)$, $\langle H_{SS} \rangle \equiv \mathrm{Tr}(\sigma H_{SS}) \sim -\beta_{SS} \mathrm{Tr}(H_{SS}^2)$, $\langle I_z \rangle \equiv \mathrm{Tr}(\sigma I_z) \sim -\beta_I \omega_I \mathrm{Tr}(I_z^2)$. In the absence of the microwave irradiation, the system is at thermal equilibrium where all three inverse temperatures are the same $\beta_S^0 = \beta_{SS}^0 = \beta_I^0$ (defined by the temperature of the environment). Since $\omega_S \gg \omega_I, \tilde{D}$ (where $\tilde{D}$ is the effective strength of the electron-electron coupling), the electron-electron and nuclear polarisations are negligibly small in comparison with the electron polarisation, $\langle H_{SS}/\tilde{D} \rangle, \langle I_z \rangle \ll \langle S_z \rangle$. The microwave irradiation creates a thermal contact between the electron Zeeman and electron-electron coupling reservoirs: the microwave irradiation energy absorbed by the electron Zeeman reservoir is transferred to the electron-electron coupling energy increasing its inverse temperature β_S and polarisation $\langle H_{SS} \rangle$. The electron-nuclear coupling creates a thermal contact between the electron-electron coupling and nuclear Zeeman reservoirs: the electron-electron coupling energy is passed on to the nuclear Zeeman energy leading to both nuclear inverse temperature and polarisation β_I, $\langle I_z \rangle$ enhancement. As a result, the electron Zeeman reservoir is "heated" while the electron-electron coupling and the nuclear Zeeman reservoirs are simultaneously "cooled" establishing new non-thermal equilibrium inverse temperatures β_S^*, β_{SS}^*, β_I^*. The dynamics of the "cooling process"

$$\beta_S^0 = \beta_{SS}^0 = \beta_I^0 \quad \longrightarrow \quad \beta_S^*, \beta_{SS}^*, \beta_I^* \tag{1}$$

is described in the microwave rotating frame by linear rate equations for the observables $\langle \Delta S_z \rangle$ (where $\Delta = \omega_S - \omega_0$ is the offset of the the microwave frequency from the electron resonance), $\langle H_{SS} \rangle$ and $\langle \omega_I I_z \rangle$ obtained purely thermodynamically involving phenomenological heat capacities and relaxation parameters of the three reservoirs.

The thermodynamic approach has a number of unsatisfactory aspects. First, in order to linearise the effective rate equations, the high-temperature approximation is required, although it is not valid at very low solid state temperatures. Second, the thermodynamic approach does not allow dynamical calculations on individual spin level necessary for a detailed description, especially in solids where spatial spin geometries play an important part resulting in more complicated pictures due to spin and spectral diffusion. Third, the thermodynamic concept does not provide any causal insight why the electron, electron-electron and nuclear ensembles can be treated in the "thermodynamic way". Besides, as evidenced by many experiments[5,16–18,22,24,28,29,31], depending on joint properties of paramagnetic impurities and nuclei as well as physical conditions, in practice several basic DNP mechanisms can simultaneously occur, so all mechanisms must be simultaneously studied and applied. This makes the development of the quantum theory of TM, along with its links to macroscopic simulations, a highly relevant problem.

The lack of the comprehensive quantum theory of TM is caused by the fact that large electron spin ensembles are involved in the TM dynamics. Such ensembles are hardly tractable either analytically or numerically. Their properties strongly depend on their geometric features and cannot be replaced by combinations of small spin systems or statistical methods based on small spin systems.

In the following work we develop a theory of TM based on purely quantum considerations. In section 2 the quantum description of a general TM DNP model is summarised, the role of asymmetry of the electron-electron coupling is discussed and eigenstates of the electron ensemble are described. We develop then a minimal 6-level microscopic model and test the theory and relate it to the thermodynamic picture. Optimal conditions for the nuclear polarisation enhancement are presented. In section 3, effects of inhomogeneous broadening of the electron paramagnetic resonance (EPR) are taken into account and macroscopic simulations of DNP spectra are performed. We demonstrate the good agreement of the suggested theory with experiments involving samples doped with BDPA or trityl free radicals.

2 Quantum theory of TM

Due to the large numbers of spins involved, it is impossible to exactly solve the problem in its full quantum notations, so a simplified qualitatively minimal model is necessary where the electron ensemble, absorbing the microwave power and acting on nuclei, is considered as a whole, without specifying its spatial geometry and the coupling values. Below, we derive such 6-level minimal quantum model, which is sufficient to fully clarify and illustrate the quantum theory of TM as well as to demonstrate its links to the thermodynamic model. We start from the general quantum description of the TM mechanism, the role of the asymmetry of electron-electron coupling and the analysis of eigenstates of the electron ensemble.

2.1 General quantum description of TM mechanism

TM DNP is observed most commonly in materials where EPR spectra of the paramagnetic impurities have a dominating homogeneous broadening. This is the case, for example, in single crystals or systems containing concentrated free radicals with negligibly small g-anisotropy and hyperfine splitting. For such systems the effective electron-nuclear spin Hamiltonian can be written in the form

$$H = \omega_I I_z + \Delta S_z + \omega_1 S_x + H_{SS} + H_{IS}.$$

Here $\mathbf{I} = \sum \mathbf{I}_k$, $\mathbf{S} = \sum \mathbf{S}_j$ are the total nuclear and electron spins, ω_I is the nuclear frequency, Δ is the offset of the microwave frequency from the centre of the EPR line, ω_1 is the microwave field strength. The terms H_{SS}, H_{IS} describe the electron-electron

and electron-nuclear interactions which are of dipole-dipole nature and are given by the secular expressions commuting with the electron Zeeman term ΔS_z

$$H_{SS} = \sum_{j<j'} D_{jj'} \left(2S_{jz}S_{j'z} - \frac{1}{2}S_j^+ S_{j'}^- - \frac{1}{2}S_j^- S_{j'}^+ \right),$$

$$H_{IS} = \frac{1}{2}\sum_{k,j} \left(B_{kj} I_k^+ + B_{kj}^* I_k^- \right) S_{jz}.$$

For simplicity we do not write out interactions between the nuclear spins which are assumed to be all of one species and spin 1/2.

Quantum mechanically, the TM mechanism can be described as follows. In solid state, the dipole-dipole spin interactions are not rotationally invariant and strongly depend on spatial orientations and lengths of interacting pairs. This means that the electron-electron part H_{SS} does not commute with the microwave $\omega_1 S_x$ and electron-nuclear H_{IS} terms, and the interaction strengths $D_{jj'}$, B_{kj} are not symmetric with respect to electron spin permutations. As a result, the combined action of H_{SS} and $\omega_1 S_x$ creates polarisation gradients between different electron spins, and the combined action of H_{SS} and H_{IS} transfers the difference in polarization between electron spins to nuclear spins.

The mechanism is most efficient at either edge of the homogeneous EPR spectrum, i.e., for $\Delta \sim \pm\bar{D}$, where $\bar{D}$ is the halfwidth of the EPR line. In the case $\Delta \sim \bar{D}$, the initially populated ground state of the electron Hamiltonian $\Delta S_z + H_{SS}$ becomes degenerate, causing a resonant exchange of populations between eigenstates of the Zeeman and electron-electron parts ΔS_z, H_{SS}. The microwave energy absorbed by the electron Zeeman part is efficiently transferred to the energy of the electron-electron coupling. Due to the presence of the nuclear Zeeman term $\omega_I I_z$, the magnitude $\bar{D}$ should not be too small compared to ω_I, so as to provide an appreciable difference between the effective frequencies $\sim \omega_I \pm \bar{D}$ of the electron-nuclear term H_{IS} in the frame of $\omega_I I_z + H_{SS}$. In this case, electron spin flip-flops induce fast nuclear spin flips leading to an efficient transfer of the energy of the electron-electron coupling to the nuclear Zeeman energy. Similarly, for $\Delta \sim -\bar{D}$, the initially populated highest energy state of $\Delta S_z + H_{SS}$ becomes degenerate, and the nuclear spins gain the same polarisation but with the negative sign. Note that for $\Delta \sim \pm\omega_I$ (and not very large $\bar{D}$) the SE mechanism occurs in the system, so both TM and SE contributions should be expected in the DNP spectrum.

2.2 Asymmetry of electron-electron coupling

As mentioned previously, the requirement of strong asymmetry of electron-electron coupling is necessary for the TM mechanism to work. This requirement consists in the fact that the coupling is anisotropic, $[H_{SS}, S_x] \neq 0$, and the distribution of the sums $d_q \equiv \sum_{q'} D_{qq'}$ (each being the sum of couplings of a given electron to all other electrons) has a strong non-zero dispersion, i.e., the magnitudes d_q are not the same but widely distributed around their average value $\bar{d}$.

To illustrate the crucial role of this asymmetry in TM, we numerically simulated a model of three interacting electrons 1, 2 and 3 and one nucleus, for simplicity interacting with only electron 1, with the standard relaxation model we used earlier[19]. Since two-electron systems are always symmetric, the three-electron model is the simplest case where the electron-electron coupling asymmetry is possible. The results are shown in Fig.1 where two cases are plotted: an asymmetric case with respect to permutations of electrons 2 and 3, $D_{12} \not\sim D_{13}$ with $d_2 \not\sim d_3$, and a symmetric case $D_{12} \sim D_{13}$ with $d_2 \sim d_3$. In both cases, we kept the same average value $\bar{d} = 0$ to have the plots symmetric with respect to the zero microwave frequency offset $\Delta = 0$. It is evident that the polarisation difference between electrons 2 and 3, strong in the asymmetric case and quenched in the symmetric case, is transferred during TM to the nucleus connected with electron 1, while the polarisation differences between electrons 1, 2 and 1, 3 are not transferred.

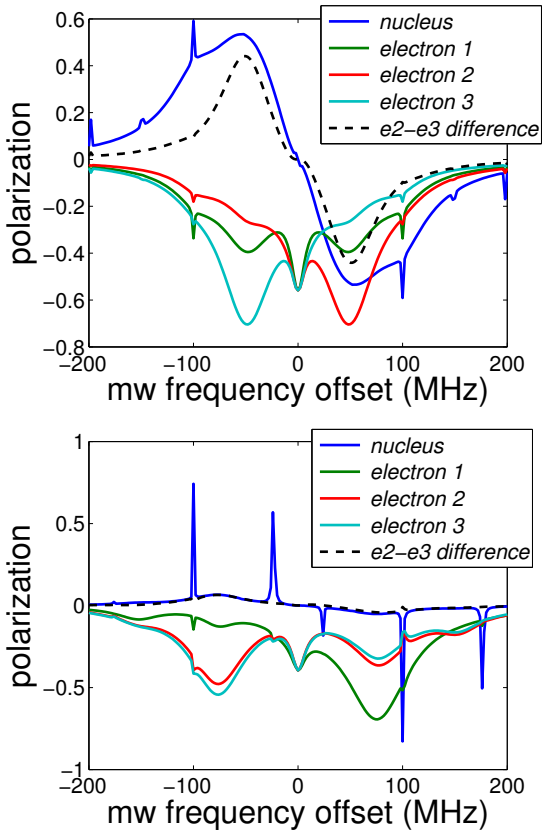

Fig. 1 The nuclear (blue) and electron (green, red and cyan) polarisations as a function of the microwave offset Δ for the model containing three electrons and one nucleus, in two situations: the strongly asymmetric case $D_{12} = -D_{13} = 40$ MHz, $D_{23} = 0$ (top) and the close to symmetric case $D_{12} = 40$ MHz, $D_{13} = 32$ MHz, $D_{23} = -72$ MHz (bottom). The narrow blue peaks correspond to SE split by the electron-electron coupling, the wide blue peaks correspond to TM. It can be seen that TM is due to the transfer of the polarisation difference between electrons 2 and 3 (dotted line), large in the asymmetric case and quenched in the symmetric case, to the nucleus connected to electron 1. Results are shown for $t = 100$ s starting from the thermal state. The system parameters are $p = 0.9$, $\omega_1 = 100$ kHz, $\omega_I = 100$ MHz, $B_1 = 1$ MHz, $T_{1e} = 1$ s, $T_{2e} = 10$ μs, $T_{1n} = 100$ s, $T_{2n} = 1$ ms.

2.3 Eigenstates of electron ensemble

The basic 3-electron model considered in the previous subsection, although illustrating the complex nature of TM and importance of the asymmetry, does not fully reflect the real situation. First, in the electron ensemble each electron spin is closely surrounded with more than two electrons, so an interplay between all possible electron polarisation gradients becomes responsible for the dynamics. Second, the distribution of the electron-electron couplings $D_{jj'}$, which essentially determine the dynamics, is different for each electron: in frozen samples and powders these couplings are randomly distributed, so their statistical properties within the whole ensemble of simultaneously interacting electrons should be considered.

At low temperatures, the thermal polarisations of the electron spins are approximately equal, and the most populated state is the Zeeman state $\chi^{(0)}$ where all electron spins are in the state "down" (or "up" depending on the chosen sign of the electron gyromagnetic ratio). The state $\chi^{(0)}$ is an eigenstate of both ΔS_z and H_{SS} with the eigenvalues $-N\Delta/2$, $d=\sum d_j/4$ respectively, where N is the number of electrons in the system and $d_j=\sum_{j'} D_{jj'}$.

Other common eigenstates of ΔS_z and H_{SS} belong to invariant subspaces $V^{(m)}$ spanned by electron Zeeman states with exactly m spins in the state "up" and $N-m$ spins in the state "down". The electron Zeeman energy ΔS_z in these subspaces equals $(m-N/2)\Delta$. The energy of the electron-electron coupling H_{SS} is distributed inside each subspace $V^{(m)}$ between some values $-D_-^{(m)}$ and $D_+^{(m)}$ depending on the strength of the electron-electron coupling. See Fig.2, top, where the structure of the (lowest) quantum states of the electron Hamiltonian is schematically depicted.

The microwave irradiation term $\omega_1 S_x$ generates an exchange of populations between the ground state $\chi^{(0)}$ and the excited eigenspaces $V^{(1)}$, $V^{(2)}$, ... For relatively small values of ω_1 and relatively large values of Δ, the most efficient exchange occurs between $\chi^{(0)}$ and the first subspace $V^{(1)}$, so the influence of the higher subspaces $V^{(m)}$, $m>1$, can be treated as negligible.

Denoting $s_q^{(1)}$ the Zeeman state with the qth electron spin in the state "up" and all other electron spins in the state "down", the operator S_x couples the ground state $\chi^{(0)}$ to the symmetric combination of $s_q^{(1)}$,

$$\chi^{(1)} \equiv S_x\chi^{(0)} = S^+\chi^{(0)}/2 = \sum_q s_q^{(1)}/2.$$

We have

$$H_{SS}s_q^{(1)} = \left(-d_q+d\right)s_q^{(1)} - \frac{1}{2}\sum_{q'\neq q} D_{qq'}s_{q'}^{(1)} \qquad (2)$$

and so

$$H_{SS}\chi^{(1)} = d\chi^{(1)} - \frac{3}{4}\sum_q \tilde{d}_q s_q^{(1)}, \quad \tilde{d}_q = d_q - \bar{d} \qquad (3)$$

where we used the facts that $d_q=\sum_{q'} D_{qq'}$ and $\bar{d}\equiv\sum d_j/N \ll d = \sum d_j/4$.

Due to the asymmetry of the electron-electron coupling (caused, for example, by defects of the crystalline lattice or geometric distortions of the frozen solution or powder), the distribution of the centralised magnitudes $\tilde{d}_q$ has a nonzero dispersion,

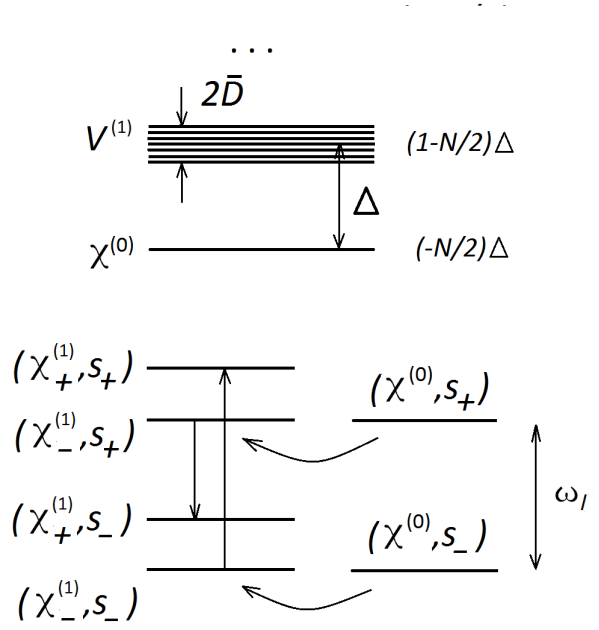

Fig. 2 *Top*: the schematic representation of the ground state $\chi^{(0)}$ and the first excited subspace $V^{(1)}$ of the electron Hamiltonian $\Delta S_z + H_{SS}$ before TM reaches its maximum, $\Delta \gg D$. At $\Delta \sim D$ the ground state becomes degenerate with $V^{(1)}$ causing a resonant exchange between the electron-electron coupling and electron Zeeman energies leading to TM. *Bottom*: the schematic representation of the TM process based on the minimal 6-level model, $\Delta \sim \bar{D} \ll \omega_I/2$. The electron Zeeman energy is transferred to the energy of the electron-electron coupling and then to the nuclear Zeeman energy. At $\bar{D}\sim\omega_I/2$, the excited product states $(\chi_+^{(1)},s_-)$, $(\chi_-^{(1)},s_+)$ become degenerate leading to the maximal nuclear polarisation enhancement.

$D' = (\sum \tilde{d}_q^2)^{1/2} > 0$. The same shift d is present in all diagonal elements of the matrix for H_{SS}. It means that $\chi^{(1)}$ is expanded into eigenstates $\chi_q^{(1)}$ of H_{SS} with energies between the values $d-\bar{D}$ and $d+\bar{D}$, where d is exactly the energy of the ground state $\chi^{(0)}$ in H_{SS} and $\bar{D}>0$ is proportional to D'. We assume for simplicity that the corresponding eigenstates are distributed symmetrically around d (Fig.2, top).

2.4 Minimal 6-level microscopic model

Suppose we are interested in polarisation of a single nuclear spin I. Then only the single term $I_x\sum B_j S_{jz}$ is present in the electron-nuclear part H_{IS}. Adding the "up" and "down" states $s_\pm$ of the nucleus, we come to the set of eigenstates $(\chi^{(0)},s_\pm)$, $(\chi_q^{(1)},s_\pm)$ of the electron-nuclear Hamiltonian $\Delta_z + H_{SS} + \omega_I I_z$ with the energies $d\pm\omega_I/2$, $d+D_q\pm\omega_I/2$ respectively, where D_q are distributed within the interval $(-\bar{D},\bar{D})$ and we let for definiteness $\omega_I>0$.

For large values of Δ, the strongest population exchange between the ground state $\chi^{(0)}$ and the first excited subspace $V^{(1)}$ corresponds to the states with the smallest energy gap, i.e., the states $(\chi^{(0)},s_\pm)$ and $(\chi_-^{(1)},s_\pm)$ where $\chi_-^{(1)}$ has the smallest energy $d-\bar{D}$ in $V^{(1)}$. The strongest population exchange between the "up" and "down" subspaces of the nucleus corresponds to the states, for which the relevant energy gap is the smallest, that is the

states $(\chi_+^{(1)}, s_-)$ and $(\chi_-^{(1)}, s_+)$, where $\chi_+^{(1)}$ has the maximal energy $d+\bar{D}$ in $V^{(1)}$. Thus, the three eigenstates $\chi^{(0)}$, $\chi_\pm^{(1)}$ of H_{SS} are the most important, and along with the two states of the nucleus we come to a 6-level minimal model describing TM. See Fig.2, bottom, where the TM process based on the 6-level minimal model is schematically shown.

The TM mechanism becomes maximally efficient when $\Delta \sim \bar{D}$ where the ground state $\chi^{(0)}$ becomes degenerate with the first excited state $\chi_-^{(1)}$ causing, via the presence of the microwave irradiation, an equilibration of their populations and a resonant exchange between the electron Zeeman and the electron-electron coupling energies. Due to the presence of the electron-nuclear coupling, an exchange between populations of the excited product states $(\chi_-^{(1)}, s_+)$, $(\chi_+^{(1)}, s_-)$ occurs resulting in transfer of population from one nuclear state s_+ to the other s_-. The opposite process $s_- \to s_+$ also simultaneously occurs but the two processes have different transition frequencies $\sim \omega_I \pm 2\bar{D}$, so one of the processes dominates. An exchange between the electron-electron coupling energy and the nuclear Zeeman energy occurs, leading to an enhancement of negative nuclear polarisation. The difference of the electron-nuclear energy $\Delta\bar{S}_z + \bar{H}_{SS} + \omega_I I_z$ between $(\chi_-^{(1)}, s_+)$ and $(\chi_+^{(1)}, s_-)$ is $\sim \omega_I - 2\bar{D}$, therefore the maximal nuclear polarisation enhancement is achieved in systems with strong electron-electron coupling, to satisfy the condition $\Delta \sim \bar{D} \sim \omega_I/2$ (Fig.2, bottom). Conversely, at $\Delta \sim -\bar{D}$, a population exchange between the ground state $\chi^{(0)}$ and the excited state products $(\chi_+^{(1)}, s_-)$, $(\chi_-^{(1)}, s_+)$ dominates instead, leading to a positive nuclear polarisation enhancement (in analogy to the zero-quantum and double-quantum "forbidden transitions" in SE).

The important characteristic parameter $\bar{D}$, responsible for the positions of TM peaks in the DNP spectrum, is comparable to the half-width of the homogeneous EPR line. Indeed, the Fourier spectrum of the operator S_x in the frame rotating with H_{SS}, $e^{iH_{SS}t} S_x e^{-iH_{SS}t}$, featuring the energy differences between $\chi^{(0)}$ and $\chi_q^{(1)} \in V^{(1)}$, belongs exactly to the interval $(-\bar{D}, \bar{D})$. The values $\pm\bar{D}$ define the edges of the homogeneously broadened (low-temperature) EPR spectrum.

The simplest realisation of the Hamiltonian is to let the microwave part $\bar{H}_{MW} = \omega_1 S_x$ couple $\chi^{(0)}$ to a symmetric combination of $\chi_\pm^{(1)}$ and let the electron contribution to the electron-nuclear part $\bar{L}_z = \sum B_j S_{jz}$ couple $\chi_-^{(1)}$ to $\chi_+^{(1)}$. Indeed, for pairs of spatially close electrons, typically $d_q - d_{q'} \sim D_{qq'}$, so non-diagonal terms of H_{SS} in the basis $\{s_q^{(1)}\}$ are not quenched, see equation (2). It means that in eigenvalues of H_{SS} the Zeeman states $s_q^{(1)}$ are strongly mixed. In particular, $\chi_\pm^{(1)} = \sum c_q^\pm s_q^{(1)}$ with some nonzero coefficients $c_q^\pm$. Hence, $2\chi^{(1)} = (\sum c_q^+)\chi_+^{(1)} + (\sum c_q^-)\chi_-^{(1)} + ...$, where, due to the symmetry of the defects d_q, we obtain $\sum c_q^+ \sim \sum c_q^-$. Nuclei remote from electrons can get their polarisation only from nuclei close to electrons via spin diffusion. Hence, it is reasonable to assume that the nucleus I is close to one of electrons, i.e., in $\bar{L}_z$ one of the strengths B_j dominates. We have $2S_j\chi_\pm^{(1)} = c_j^\pm s_j^{(1)} - \sum_{j'\neq j} c_{j'}^\pm s_{j'}^{(1)}$. Since $\chi_\pm^{(1)}$ are orthogonal and normalised, we obtain $2S_{jz}\chi_\pm^{(1)} = c_j^+ c_j^- \chi_\mp^{(1)} + ...$, so $\bar{L}_z$ indeed symmetrically mixes the eigenstates $\chi_\pm^{(1)}$. The states $\chi^{(0)}$, $\chi_\pm^{(1)}$ are eigenstates of the electron and electron-electron parts ΔS_z, H_{SS}, the ground state $\chi^{(0)}$ is an eigenstate of $\bar{L}_z$. Keeping the only informative traceless parts of S_z, H_{SS} and utilizing the Hermitian form of the Hamiltonian, we come to the representation of the electron ensemble by a 3-level quantum system with the matrix expressions in the basis $\chi^{(0)}$, $\chi_-^{(1)}$, $\chi_+^{(1)}$

$$\Delta\bar{S}_z = \frac{\Delta}{2}\begin{pmatrix} -N & 0 & 0 \\ 0 & 2-N & 0 \\ 0 & 0 & 2-N \end{pmatrix} \longrightarrow \frac{\Delta}{3}\begin{pmatrix} -2 & 0 & 0 \\ 0 & 1 & 0 \\ 0 & 0 & 1 \end{pmatrix},$$

$$\bar{H}_{SS} = \begin{pmatrix} d & 0 & 0 \\ 0 & d-\bar{D} & 0 \\ 0 & 0 & d+\bar{D} \end{pmatrix} \longrightarrow \bar{D}\begin{pmatrix} 0 & 0 & 0 \\ 0 & -1 & 0 \\ 0 & 0 & 1 \end{pmatrix},$$

$$\bar{L}_z = \frac{1}{2}\begin{pmatrix} -b_1 & 0 & 0 \\ 0 & 0 & b_2 \\ 0 & b_2 & 0 \end{pmatrix}, \quad \bar{H}_{MW} = \bar{\omega}_1\begin{pmatrix} 0 & 1 & 1 \\ 1 & 0 & 0 \\ 1 & 0 & 0 \end{pmatrix}.$$

Here $b_1 \sim \sum B_j$, the magnitude b_2 characterises the length of the projection of $\bar{L}_z\chi_-^{(1)}$ to $\chi_+^{(1)}$ and depends on the electron-nuclear interaction strengths B_j as well as statistics of the distribution $\{d_q\}$, $\bar{\omega}_1$ is the effective microwave power proportional to ω_1 but depending also on $\bar{D}$ because the latter defines the contributions of the states $\chi_\pm^{(1)}$ to $\chi^{(1)} = S_x\chi^{(0)}$. Below we treat $b_{1,2}$ and $\bar{\omega}_1$ as independent effective "fitting" parameters. For further details see the next section and the considerations around the generalised equations (5), (6). Adding the two nuclear states "up" and "down" $s_\pm$ with the standard 2-level nuclear operators

$$I_z = \frac{1}{2}\begin{pmatrix} -1 & 0 \\ 0 & 1 \end{pmatrix}, \quad I^+ = (I^-)^* = \begin{pmatrix} 0 & 1 \\ 0 & 0 \end{pmatrix},$$

we obtain finally a 6-level quantum system with the Hamiltonian

$$H = \omega_I I_z + \Delta\bar{S}_z + \bar{H}_{MW} + \bar{H}_{SS} + I_x\bar{L}_z.$$

To take thermal spin relaxation into account, we note that at a low temperature thermal equilibrium the electron spins are approximately equally polarised, and the population of the ground state $\chi^{(0)}$ equals $\left(\frac{1+p}{2}\right)^N$ while the populations on the first excited subspace $V^{(1)}$ equal $\frac{1-p}{2}\left(\frac{1+p}{2}\right)^{N-1}$ where $p = \tanh\frac{\hbar|\omega_S|}{2kT} \in (0,1)$. Even at low temperatures, the nuclear polarisation is negligibly small compared to p. It means that, up to a scaling factor and the requirement of trace 1, the initial thermal density operator in the basis $\chi^{(0)}$, $\chi_-^{(1)}$, $\chi_+^{(1)}$ is written as

$$\sigma_0 = \frac{1}{3-p}\begin{pmatrix} 1+p & 0 & 0 \\ 0 & 1-p & 0 \\ 0 & 0 & 1-p \end{pmatrix}.$$

In the thermal electron relaxation back to the state σ_0 the most effective are spontaneous jumps between the excited states $\chi_\pm^{(1)}$ and the ground state $\chi^{(0)}$ reducing the microwave excitation of the latter. For the thermal nuclear relaxation, jumps between the "up" and "down" states are the most important. Assuming that

these quantum jump processes are of Markovian nature, we come to the Lindblad form of the relaxation superoperator

$$\hat{\Gamma} = \sum_{s=1,2} \left[R_1^+ \hat{D}(\bar{K}_s^+) + R_1^- \hat{D}(\bar{K}_s^-) + R_2 \hat{D}(\bar{K}_{sz}\right] +$$

$$+ r_1 \left[\hat{D}(I^+) + \hat{D}(I^-)\right] + r_2 \hat{D}(I_z),$$

where the standard notation for the dissipator is used

$$\hat{D}(X)\sigma = X\sigma X^* - \frac{1}{2}\left(X^* X\sigma + \sigma X^* X\right),$$

the operators $K_{sz}, K_s^{\pm}$ are given by the matrix expressions

$$K_{1z} = \frac{1}{2}\begin{pmatrix} 1 & 0 & 0 \\ 0 & -1 & 0 \\ 0 & 0 & 0 \end{pmatrix}, \quad K_1^+ = (K_1^-)^* = \begin{pmatrix} 0 & 1 & 0 \\ 0 & 0 & 0 \\ 0 & 0 & 0 \end{pmatrix},$$

$$K_{2z} = \frac{1}{2}\begin{pmatrix} 1 & 0 & 0 \\ 0 & 0 & 0 \\ 0 & 0 & -1 \end{pmatrix}, \quad K_2^+ = (K_2^-)^* = \begin{pmatrix} 0 & 0 & 1 \\ 0 & 0 & 0 \\ 0 & 0 & 0 \end{pmatrix},$$

and the rates are proportional to the corresponding longitudinal and transversal relaxation rates,

$$R_1^{\pm} = \frac{1 \pm p}{2T_{1e}}, \quad R_2 = \frac{2}{T_{2e}}, \quad r_1^{\pm} = \frac{1}{2T_{1n}}, \quad r_2 = \frac{2}{T_{2n}}.$$

The dynamics of the density operator is described then by the master equation

$$\dot{\sigma} = -i[H, \sigma] + \hat{\Gamma}\sigma$$

with the initial state being the thermal state $\sigma(0) = \sigma_0$.

In Fig.3, the evolution of the steady-state nuclear (blue) and electron (green) DNP spectra of the minimal model from the dominating SE to strong TM is shown for increasing electron-electron coupling $\bar{D}$ while other system parameters are kept fixed. It is evident that at $\Delta \sim \pm\bar{D}$ there is a resonant transfer of the absorbed microwave energy to the nucleus due to TM. The maximal nuclear polarisation enhancement is observed at $\pm\Delta \sim \bar{D} \sim \omega_I/2$ as described. In this optimal case the nuclear polarisation has also the shortest build-up time.

To illustrate the link to the thermodynamic model and the "cooling process" (1), in Fig.4, the steady-state DNP spectra (blue), the relative electron depolarisation $(\langle\bar{S}_z\rangle - \langle\bar{S}_z\rangle_0)\Delta/\omega_I$ (green) and the relative polarisation of the electron-electron coupling $\langle\bar{H}_{SS}\rangle/\omega_I$ (red) are plotted for the same four values of $\bar{D}$ with the same system parameters as in Fig.3. All three curves have peaks near the same value $\Delta \sim \pm\bar{D}$, which means that maximal TM corresponds to the simultaneously resonant exchange between the nuclear Zeeman energy, electron-electron coupling energy and electron Zeeman energy absorbed from the microwave: the electron Zeeman reservoir is "heated" while the electron-electron coupling and the nuclear Zeeman reservoirs are simultaneously "cooled" in good agreement with the thermodynamic model. It is seen in Fig. 4 that for increasing $\bar{D}$ the electron depolarisation and electron-electron coupling polarisation tend to equalise, establishing a "temperature balance", i.e., for strong electron-electron coupling in the "cooling process" (1) the inverse temperatures β_S, β_{SS} behave in such way that the magnitude $\mathrm{Tr}(\sigma H_0) \equiv \Delta\langle S_z\rangle + \langle H_{SS}\rangle$ is an integral of motion with the same steady-state value as in the thermal state: $\langle H_{SS}\rangle + \Delta\langle S_z\rangle = \langle S_z\rangle_0$, as might be expected from the thermodynamic model[13]. The nuclear polarisation is comparable with the other two for small values of $\bar{D}$, becomes larger than those for intermediate values and becomes smaller than those for large values of $\bar{D}$.

The nuclear polarisation arising from TM strongly depends on the strength of the effective electron-nuclear coupling parameter b_2 showing a nonlinear behaviour with a certain optimal value where the TM peaks are maximal. Since b_2 is proportional to the reciprocal cube of the electron-nuclear distance, nuclei very close to electrons or remote far away from them are less polarised — a phenomenon observed also in the SE and CE cases[19,20]. This is explained by the fact that strong values of B_j and the presence of single-quantum nuclear coherences in the operator H_{IS} cause an additional saturating effect on the nuclear polarisation. Small values of B_j are not sufficient for enabling an efficient transfer of the nuclear polarisation from the electrons. Decreasing/increasing the microwave field strength $\bar{\omega}_1$ leads to narrowing/broadening of the TM peaks, preserving their positions and heights. There are also nonlinear dependencies of heights and widths of the TM peaks on the ratio $\bar{D}/\omega_I$ and the spin relaxation rates.

3 Macroscopic simulations and links to experiments

The microscopic theory developed in the previous sections is directly applicable to macroscopic calculations in cases where the EPR line has a negligible inhomogeneous contributions: for example, single crystals or free radicals with a very small g-anisotropy. We can assume here that each electron spin belongs to a single spin frequency package and transfers its polarisation to a bulk nucleus in a manner defined by the minimal model .

Among such radicals, the most commonly used is the α,γ-bisdiphenylene-β-phenylallyl abbreviated shortly as BDPA. Indeed, TM DNP has been observed for the first time in m-xylene doped with BDPA at cryogenic temperatures ~ 0.5 K and a static field of 2.5 T. Strong SE and TM contributions to the proton DNP spectrum were simultaneously observed[24]. To simulate the experimental DNP profile, i.e., the dependence of the proton polarisation $p_n(\Delta)$ on the offset Δ of the microwave frequency from the centre of the EPR spectrum, we used the simple linear combination formula

$$p_n(\Delta) = c_1 p_n^{(SE)}(\Delta) + c_2 p_n^{(TM)}(\Delta)$$

accounting for solid effect and TM contributions.

For 2.5 T the proton frequency is $\omega_I \sim 106$ MHz, and the EPR line $g(\omega)$ can be simulated as a single Lorentzian spin package of half-width $D \sim 10$ MHz. Since $D \ll \omega_I$, there are no appreciable CE contributions, and the normalised SE shape of the DNP spectrum can be simulated as

$$p_n^{(SE)}(\Delta) = g(\Delta + \omega_I) - g(\Delta - \omega_I), \quad g(\omega) = \left(1 + \frac{\omega^2}{D^2}\right)^{-1}. \quad (4)$$

To simulate the TM shape, we applied our minimal model where we chose $\bar{D}$ comparable with the basic half-width of the EPR line.

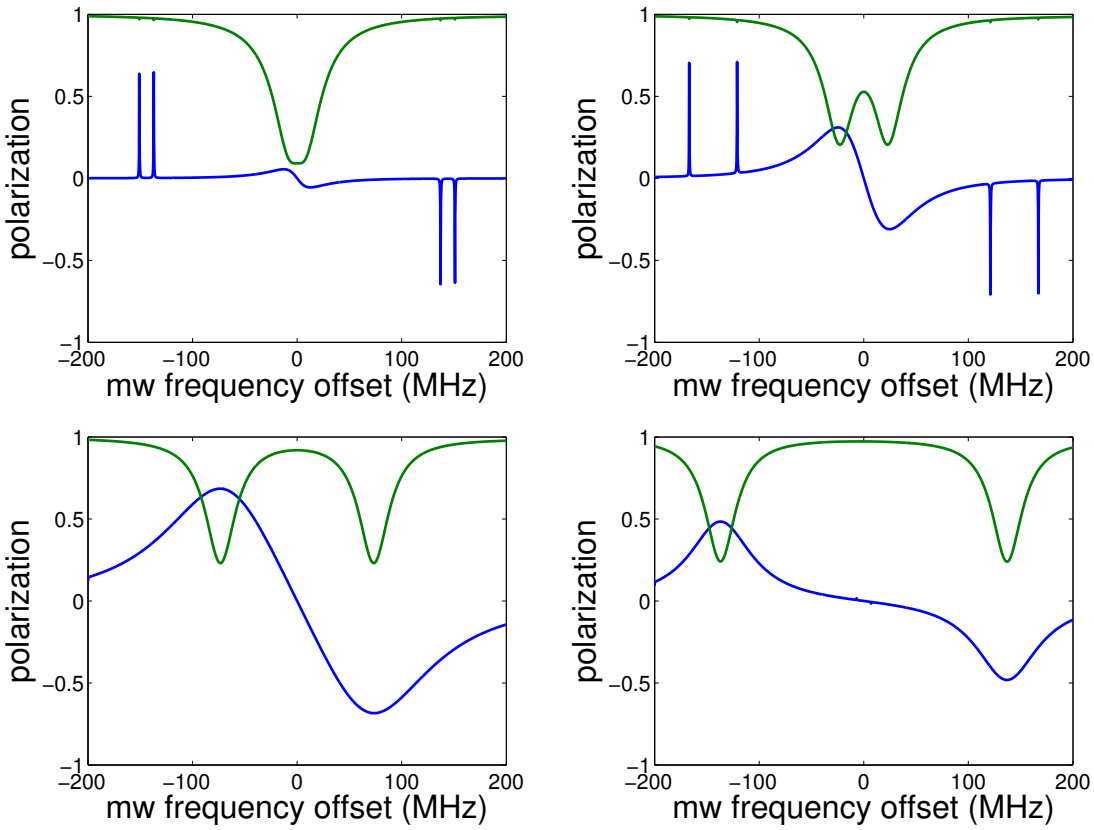

Fig. 3 The transition of the nuclear (blue) and electron (green) DNP spectra of the minimal model from the dominating SE to strong TM with increasing electron-electron coupling $\bar{D} = 7$ MHz (top left), $\bar{D} = 23$ MHz (top right), $\bar{D} = 72$ MHz (bottom left) and $\bar{D} = 137$ MHz (bottom right). The narrow blue peaks correspond to SE split by the electron-electron coupling $\Delta \sim \omega_I \pm \bar{D}, -\omega_I \pm \bar{D}$, the wide peaks $\Delta \sim \pm\bar{D}$ correspond to TM. The green narrow peaks are due to transfer of the absorbed microwave energy to the nucleus during TM. The calculation is after $t = 100$ s starting from the thermal state σ_0. The system parameters are $p = 1$, $\bar{\omega}_1 = 50$ kHz, $\omega_I = 144$ MHz, $b_1 = b_2 = 0.5$ MHz, $T_{1e} = 1$ s, $T_{2e} = 10$ μs, $T_{1n} = 100$ s, $T_{2n} = 1$ ms.

The results are shown in Fig.5 where we chose $c_1 = 1.1$, $c_2 = 1$ and compared the simulated DNP spectrum with the normalised experimental one $p_{n,exp}(\Delta)/\max p_{n,exp}$. The relaxation rates were chosen typical for low temperature experiments ($T_{1e} = 1$ s, $T_{2e} = 10$ μs, $T_{1n} = 100$ s, $T_{2n} = 1$ ms) and the parameters b_1, b_2 and $\bar{\omega}_1$ were adjusted to get the best fit with the experimental data. The plot presented shows a good agreement with the experiment.

Unlike BDPA, most free radicals have an appreciably anisotropic electron g-tensor. At high magnetic fields, in frozen samples doped with such radicals, due to powder averaged spatial orientations of g, the EPR spectrum receives strong inhomogeneous broadening. The minimal model developed in the previous section cannot be directly applied to macroscopic simulations in this case, and an expansion allowing for the inhomogeneous broadening is required.

Ignoring for simplicity effects of hyperfine splitting of the electron spectrum, we have to add to the initial Hamiltonian the g-anisotropy term

$$H_{IB} = \sum_j \Delta_j S_{jz}, \quad \sum_j \Delta_j = 0$$

where Δ_j are deviations of the electron frequencies from the average offset Δ. The symmetrised electron Zeeman Hamiltonian ΔS_z does not change, while the electron-electron coupling Hamiltonian changes to $\tilde{H}_{SS} = H_{SS} + H_{IB}$. In the basis, where the two Hamiltonians are diagonal, $\tilde{H}_{SS}$ has again the energy d in the ground state $\chi^{(0)}$ (since Δ_j are centred around zero), while equations (2), (3) change to

$$H_{SS} s_q^{(1)} = \left(-d_q + \Delta_q + d\right) s_q^{(1)} - \frac{1}{2} \sum_{q' \neq q} D_{qq'} s_{q'}^{(1)} \tag{5}$$

and so

$$H_{SS} \chi^{(1)} = d\chi^{(1)} - \frac{3}{4} \sum_q \left(\tilde{d}_q - \Delta_q\right) s_q^{(1)}. \tag{6}$$

It is seen from the above formulas that packages of electron spins with similar inhomogeneous shifts Δ_q tend to behave in the same way as a single spin package but with the energies of the states $\chi_\pm^{(i)}$ shifted as $d + \Delta_q \pm \bar{D}$ where $\bar{D} \sim \max|d_q|$, defined by the same defects of the lattice, is similar for all packages. For a package with a shift $\bar{\Delta}$, the traceless operator $\bar{H}_{SS}$ is modified as

$$\bar{H}_{SS} = \begin{pmatrix} d & 0 & 0 \\ 0 & d - \bar{D} + \bar{\Delta} & 0 \\ 0 & 0 & d + \bar{D} + \bar{\Delta} \end{pmatrix} \quad \longrightarrow$$

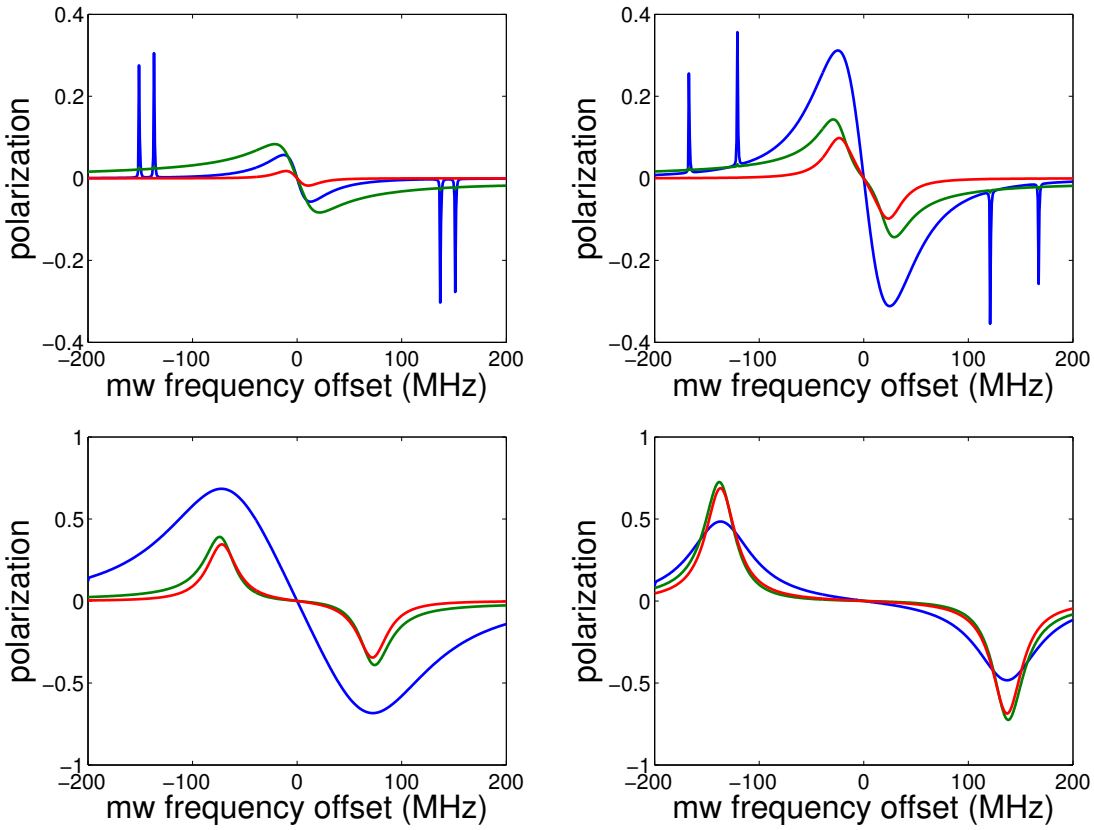

Fig. 4 The DNP spectrum (blue), the relative electron depolarisation $(\langle \bar{S}_z \rangle - \langle \bar{S}_z \rangle_0)\Delta/\omega_I$ (green) and the relative polarisation of the electron-electron coupling $\langle \bar{H}_{SS} \rangle/\omega_I$ (red) for $\bar{D} = 7$ MHz (top left), $\bar{D} = 23$ MHz (top right), $\bar{D} = 72$ MHz (bottom left) and $\bar{D} = 137$ MHz (bottom right). The calculation time and system parameters are the same as in Fig.3. All three curves have peaks near the same value $\Delta \sim \pm\bar{D}$, so the maximal TM corresponds to the simultaneously intensive exchange between all three energies, in good agreement with the thermodynamic model. For increasing $\bar{D}$ the electron depolarisation and electron-electron coupling polarisation tend to equalise. The nuclear polarisation is comparable with the other two for small values of $\bar{D}$, becomes larger than those for intermediate values and becomes smaller than those for large values of $\bar{D}$.

$$\begin{pmatrix} -2\bar{\Delta}/3 & 0 & 0 \\ 0 & -\bar{D}+\bar{\Delta}/3 & 0 \\ 0 & 0 & \bar{D}+\bar{\Delta}/3 \end{pmatrix}.$$

Comparing this with the formula for the traceless operator $\bar{S}_z$, it is obvious that the minimal model is modified by the simple shift $\Delta \to \Delta + \bar{\Delta}$.

The number of nuclei in close vicinities to electrons from each package is proportional to the numbers of electrons in the packages defined by the inhomogeneous component of the EPR spectrum. Since electron spins from packages with similar shifts $\bar{\Delta} \sim \bar{\Delta}'$ still interact with each other, each package contributes to the total TM DNP profile with a certain weight $g_{IB}(\bar{\Delta})$, where the centralised profile g_{IB} characterises the inhomogeneous component of the EPR line with some broadening caused by the interactions between the electron spin packages. Hence, we come to the averaged formula for the total TM DNP spectrum

$$p_n^{(TM)}(\Delta) = \int_{-\infty}^{+\infty} g_{IB}(\bar{\Delta})\bar{p}_n^{(TM)}(\Delta+\bar{\Delta})\,d\bar{\Delta} = \\ = \int_{-\infty}^{+\infty} g_{IB}(\bar{\Delta}-\Delta)\bar{p}_n^{(TM)}(\bar{\Delta})\,d\bar{\Delta}, \qquad (7)$$

where $\bar{p}_n^{(TM)}$ is the TM profile calculated by the minimal model and g_{IB} is normalised as $\int g_{IB}(\omega)\,d\omega = 1$.

The effect of such averaging is broadening and loss of the polarisation enhancement in comparison with a single electron frequency package — a result of the diffusion over all possible shifts $\bar{\Delta}$ generated by different electron packages. For wide shapes g_{IB}, the effective weights participating in the averaging are so small that the TM enhancement becomes negligible: large inhomogeneous broadening tends to quench the TM mechanism giving rise to CE instead.

The powder average inhomogeneous broadening of the electron resonance line can be estimated using the principal components g_s $(s = 1,2,3)$ of the g-tensor, in the standard way described, for example, in[32]. The anisotropy of g generates a powder average shape $g_0(\omega)$ characterising the distribution of electron frequencies over all possible spatial g-orientations. This distribution must then be again broadened by a homogeneous distribution $g_{HB}(\omega)$ leading to the convolution formula for the EPR line

$$g_{IB}(\omega) = \int_{-\infty}^{+\infty} g_0(\omega')g_{HB}(\omega-\omega')\,d\omega'. \qquad (8)$$

For an axially symmetric g-tensor, $g_1 < g_2 = g_3$, the shape g_0 is

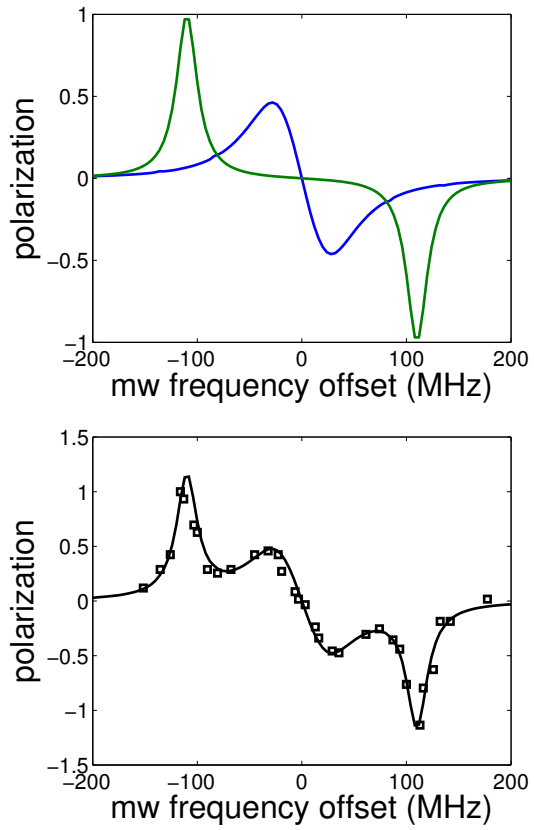

Fig. 5 *Top*: the simulated SE $p_n^{(SE)}$ (green) and TM $p_n^{(TM)}$ (blue) shapes for a Lorentzian EPR line with $D = 12$ MHz, $\tilde{D} = 27.5$ MHz, $\bar{\omega}_1 = 40$ kHz, $\omega_I = 110$ MHz and the other parameters the same as in Fig.3. *Bottom*: the simulated DNP spectrum $1.1p_n^{(SE)} + p_n^{(TM)}$ (solid line) and normalised experimental data (squares) for the proton spectrum of *m*-xylene doped with BDPA, from [24].

explicitly calculated as

$$g_0(\omega) = c\nu\left(g_2^2 - \nu^2\right)^{-1/2}, \quad \omega = \frac{\omega_e \nu}{2}, \quad g_1 < \nu < g_2$$

where c is a normalising factor, ω_e is the electron frequency at the centre of the spectrum, and g_0 is zero for ν outside the interval (g_1, g_2). In most cases, the homogeneous broadening shape g_{HB} is well approximated by a Lorentzian or Gaussian profile.

On an intermediate position between radicals with very weak and very strong g-anisotropies is the well-known triphenylmethyl radical (trityl). For this radical, as in the BDPA case, simultaneous SE and TM contributions should be observed, with the difference that the TM mechanism is now modified due to the appreciable inhomogeneous broadening. This is indeed confirmed by the experimental data below. We prepared tris(8-deutero-2,2,6,6-tetramethylbenzo[1,2-*d*;4,5-*d*']bis[1,3]dithiol-4-yl)methyl (D_3-trityl) from tris(8-deutero-2,2,6,6-tetramethylbenzo[1,2-*d*;4,5-*d*']bis[1,3]dithiol-4-yl)methanol by adapting the literature methods for the synthesis of tris(8-ethoxycarbonyl-2,2,6,6-tetramethylbenzo[1,2-*d*;4,5-*d*']bis[1,3]dithiol-4-yl)methyl.[33,34] Tris(8-deutero-2,2,6,6-tetramethylbenzo[1,2-*d*;4,5-*d*']bis[1,3]dithiol-4-yl)methanol was synthesised by adapting the literature methods for the synthesis of tris(8-ethoxycarbonyl-2,2,6,6-tetramethylbenzo[1,2-*d*;4,5-*d*']bis[1,3]dithiol-4-yl)methanol using D_4-methanol in place of diethyl carbonate.[33,34].

The experiments were performed with 15 mM D_3-trityl solutions in tetrahydrofuran (THF):toluene (2:1) frozen to a temperature of ~ 1.5 K, in static magnetic field of 3.4 T and a low microwave power $\omega_1 \sim 5$ kHz. The spectrum was obtained as follows. The sample was sonicated for 20 min to aid dissolution of the radical. Before transfer to the sample cup, the solution was visually inspected for any residue of undissolved racial. The sample (~ 70 μl) was rapidly frozen by inserting it in a pre-cooled cryostat ($T \sim 2K$). Following that, the temperature was equilibrated at $T = 1.4$ K for ~ 30 min and the measurement was started. Each point of the sweep spectrum was obtained by irradiation at a given microwave frequency for 120 s and reading the magnetization with a $\pi/2$ pulse. Before each measurement a train of 64 $\pi/2$ pulses was used to destroy the polarization. The amplitude of the signal was obtained by integrating the real part of the spectrum. All measurements were done using a home built DNP polariser connected to a commercial Bruker console for the NMR control[35]. SE and TM peaks were observed in the proton DNP spectrum (Fig.6, top). To simulate the DNP spectra, we note that the g-tensor of D_3-trityl is very close to an axially symmetric tensor with principal components $g_1 \sim 2.002$, $g_2 = g_3 \sim 2.003$. As earlier described in this section, we modelled the EPR line $g(\omega)$ using a Gaussian homogeneous broadening g_{HB} by equation (8) and applied then the same standard formula as in (4) for the SE shape, with the normalisation $g = \pm 1$ at the peak points. To simulate the TM shape $p_n^{(TM)}$, we used the minimal model and chose a shifted Gaussian inhomogeneous shape g_{IB} in equation (7). In Fig.6, bottom, the combined DNP spectrum $c_1 p_n^{(SE)} + c_2 p_n^{(TM)}$ is plotted with $c_1 = 1$, $c_2 = 3$, compared with the experimentally obtained normalised proton DNP profile $p_{n,exp}/\max p_{n,exp}$ for the D_3-trityl derivative shown in Fig.6, top. A good agreement with the experimental data is evident.

4 Conclusions

We have demonstrated that the TM DNP mechanism can be described from the purely quantum point of view, without making additional thermodynamic assumptions. First, we explain the energy exchange between the electron Zeeman and electron-electron coupling parts of the Hamiltonian. We give a full quantum description of the underlying Provotorov saturation theory, which as we show requires asymmetric distributions of electron-electron couplings for this mechanism to work. Second, we describe quantum mechanically how the electron-electron coupling energy is further transferred to nuclei, using asymmetry in the electron-nuclear coupling part of the Hamiltonian. To test the quantum theory and relate it to the thermodynamic picture, we set up a minimal 6-level model microscopic system and used our theory to calculate DNP spectra that were compared with experimental data. The optimal conditions for the nuclear polarisation enhancement were pointed out based on the minimal model. We have shown how this model can be used in macroscopic simulations and generalised to polarising agents with appreciable inho-

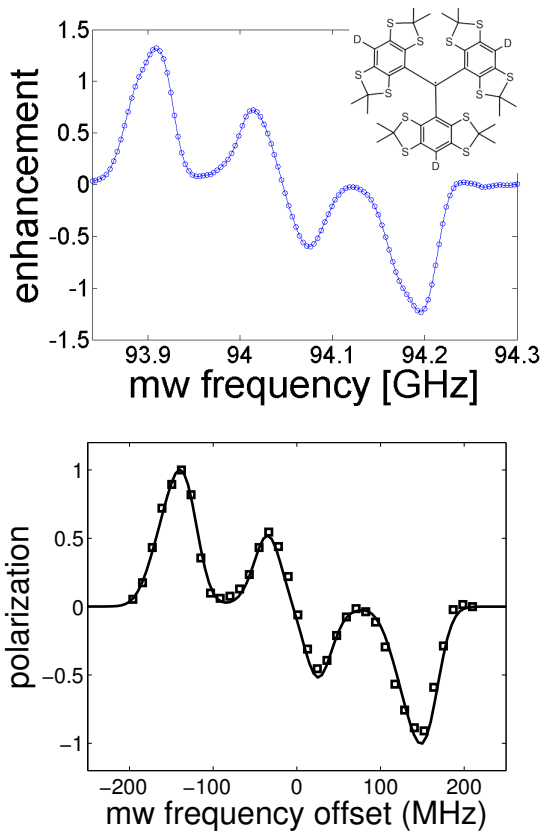

Fig. 6 *Top:* the experimental proton polarisation enhancement (in arbitrary units) of THF:toluene doped with D_3-trityl (inset). A strong mixture of SE and TM contributions is observed. *Bottom*: the simulated DNP spectrum $p_n^{(SE)}+3p_n^{(TM)}$ (solid line) compared to normalised experimental data (squares) for the proton spectrum shown on the top. The parameters used are $g_1=2.002$, $g_2=g_3=2.003$, $\omega_e=94$ GHz, $g_{HB}=\exp(-\omega^2/D_{HB}^2)$, $g_{IB}=\exp(-(\omega+f)^2/D_{IB}^2)$ with $D_{HB}=22$ MHz, $D_{IB}=20$ MHz, $f=5$ MHz, $\bar{\omega}_1=5$ kHz, $\bar{D}=30$ MHz, $b_1=b_2=1$ MHz. The other parameters are the same as in Fig.3.

mogeneous broadening of the EPR line caused by g-anisotropy. We have checked the quantum TM theory against experimental data and demonstrated the good agreement between the theory and experiment in the cases of the BDPA and trityl free radicals. This will help to develop a comprehensive theory of DNP in solids. The following final remarks are to summarise the essentials of the results obtained and the advantages of the approach developed in this work.

The underlying cause of TM is symmetry breaking, which manifests itself in two aspects featuring the solid state nature of the mechanism. First, the asymmetries caused either by intrinsic defects in crystals or random locations of electron spins in a frozen sample or powder lead to a strong dispersion of the magnitudes $d_q=\sum_{q'}D_{qq'}$ (proportional also to the concentration of the paramagnetic impurities). As a result, the microwave irradiation part of the Hamiltonian couples the ground state $\chi^{(0)}$ to a state $\chi^{(1)}$, non-trivially expanded via the eigenstates of the electron-electron part H_{SS} of the Hamiltonian. For this crucial reason, not mentioned in thermodynamic descriptions, the microwave energy absorbed by the electron ensemble is distributed into the energy of electron-electron coupling. In the symmetric case where d_q's are equal, $\chi^{(1)}$ is an eigenstate of H_{SS} with the same energy as the ground state, so TM is strongly restricted to the area $\Delta\sim 0$. This might well explain our experiments with D_3-trityl (Fig.6) where strong TM components can be attributed to chemical properties of the (weakly polar aprotic) THF:toluene solvent (chosen because D_3-trityl is not water-soluble) which, after dissolving D_3-trityl and freezing, creates a strongly asymmetric matrix. The matrix of the (highly polar protic) water:glycerol solvent is much more symmetric due to strong intermolecular forces caused by hydrogen bonding[36], so TM peaks are not observed for the (water-soluble) OX063-trityl. The same refers to the experiments with m-xylene doped with BDPA (Fig.5) compared, for example, with a Nd^{+3}-incorporated single crystal of the lanthanum magnesium double nitrate (LMN)[6,24,25]. An additional asymmetry is induced by inhomogeneous broadening of the EPR line considered in Section 3. Second, the electron-nuclear interaction Hamiltonian H_{IS} is strongly asymmetric with respect to electron spin permutations causing mixing the eigenstates of H_{SS} by H_{IS}, which in their turn are strong mixtures of Zeeman states, resulting in a transfer of the energy of electron-electron coupling to nuclei. The H_{IS} asymmetry is strongly manifested for nuclei close to electrons, so they are directly polarised by TM (and transfer then their polarisation to nuclei remote from electrons via spin diffusion). The minimal 6-level model we have suggested clearly reflects and exploits these important features. As follows from considerations in Subsection 2.2, TM is essentially a more than two-electron process where polarisation differences between electrons 2, 3 (which are even not necessarily connected, Fig.1) are transferred to polarisation of a nucleus connected to electron 1. Thus, TM is a mechanism, fundamentally different from the SE and CE mechanisms where either single electrons or pairs of electrons, interacting with nuclei, are sufficient. To avoid terminological ambiguities, we stress here that TM considered in this work is related to processes, described by quantum models involving at least three electrons. Moreover, we rather consider the electron ensemble as a whole, without specification of its concrete geometric properties and effective numbers of spins, locally involved in the dynamics. The latter was possible before only within the thermodynamic picture. Our model solves this problem purely quantum mechanically.

Despite an obvious analogy between TM and CE where electron spin polarisation differences are strongly involved in the dynamics, in the CE case large electron polarisation differences are created by a dominating inhomogeneous broadening of the EPR line (caused by a strong g-anisotropy and hyperfine splitting), and the maximal effect is observed for EPR linewidths comparable with or larger than the nuclear Larmor frequency. In the case of TM, the electron polarisation differences are due to a strong homogeneous broadening (caused by anisotropic and asymmetric dipole-dipole interelectron coupling), and the effect is already observed for EPR linewidths much less than the magnitude of ω_I. The transition from TM to CE is realised by a strong dispersion of the electron Larmor frequencies due to inhomogeneous broadening of the EPR line. This is described in Section 3 where the minimal model was modified to accommodate the simultaneous existence of many electron spin packages. In this case, the

frequency shift differences $\Delta_q - \Delta_{q'}$ tend to quench the electron-electron coupling, so the latter can be treated as a perturbation of the same order as the microwave and electron-nuclear parts of the Hamiltonian, and the resonance condition $2\bar{D} \sim \omega_I$ takes the combinational form $\Delta_q - \Delta_{q'} \sim \omega_I$, leading to the CE case where the model of electron-electron-nucleus triple spin flips is sufficient to effectively describe the dynamics.

The minimal 6-level quantum model of TM that we developed is remarkably simple, easy for simulations, in good quantitative agreement with experimental data, well describes qualitative and optimal properties of TM DNP and its links with the thermodynamic picture. The model can be extended in the future to include more than one nuclear species and/or additional paramagnetic effects. Formally, it is equivalent to a model of a single nuclear spin $I = 1/2$ interacting with a fictitious spin $L = 1$ representing the electron ensemble, with the states $\chi^{(1)}_{0,\pm}$ standing for the "zero", "up" and "down" states. Here the electron-electron coupling is equivalent to the Zeeman splitting of L, $H_{SS} \sim L_z$, while the electron Zeeman Hamiltonian is represented effectively as the zero field splitting, $S_z \sim L_z^2 - 2/3$. Since the electron-nuclear Hamiltonian H_{IS} mixes the "up" and "down" states of $L = 1$, the spin interaction here is of a nonlinear nature featuring effective terms like $I_x \left(L^{\pm}\right)^2$, impossible in interactions of dipole-dipole type. It would be interesting to find other physical applications of this basic model.

5 Acknowledgments

The research leading to these results has received funding from the EPSRC (EP/I027254 and EP/I036702) and the European Research Council under the European Union's Seventh Framework Programme (FP/2007-2013)/ERC, Grant Agreement No. 335266 (ESCQUMA).

References

1 *High field dynamic nuclear polarization — The renaissance: Special Issue, PCCP*, 2010, **12**, 5725–5928.

2 *The Different Magnetic Resonance Communities Join Forces for Progress in DNP: Special Issue, Appl. Magn. Reson.*, 2012, **43**, 1–310.

3 S. Goertz, W. Meyer and G. Reicherz, *Progr. Part. Nucl. Phys.*, 2002, **49**, 403–489.

4 K. Golman, R. Zandt, M. Lerche, R. Pehrson and J. H. Ardenkjaer-Larsen, *Cancer Res.*, 2006, **66**, 10855–10860.

5 V. A. Atsarkin, *Sov. Phys. Uspekhi*, 1978, **21**, 725–745.

6 C. D. Jeffries, *Dynamic Nuclear Orientation*, Interscience Publishers, New York, 1963.

7 D. T. Peat, A. J. Horsewill, W. Köckenberger, A. J. Perez Linde, D. G. Gadian and J. R. Owers-Bradley, *PCCP*, 2013, **15**, 7586–7591.

8 A. Abragam, *Principles of Nuclear Magnetism*, University Press, Oxford, 1982.

9 A. Abragam and W. G. Proctor, *C. R. Acad. Sci.*, 1958, **246**, 2253–2256.

10 A. Kessenikh, V. Luschikov and A. Manenkov, *Sov. Phys. Solid State*, 1963, **8**, 835–837.

11 C. F. Hwang and D. A. Hill, *Phys. Rev. Lett.*, 1967, **19**, 1011–1014.

12 K. N. Hu, H. H. Yu, T. M.Swager and R. G. Griffin, *J. Am. Chem. Soc.*, 2004, **126**, 10844–10845.

13 B. N. Provotorov, *Sov. Phys. JETP*, 1962, **14**, 1126–1131.

14 M. Borghini, *Phys. Rev. Lett.*, 1968, **20**, 419.

15 V. A. Atsarkin and M. I. Rodak, *Sov. Phys. Uspekhi*, 1972, **15**, 251–265.

16 T. Can, M. Caporini, F. Mentink-Vigier, B. Corzilius, J. J. Walish, M. Rosay, W. E. Maas, M. Baldus, S. Vega, T. M. Swager and R. Griffin, *J. Chem. Phys.*, 2014, **141**, 064202.

17 Y. Hovav, A. Feintuch and S. Vega, *J. Magn. Reson.*, 2010, **207**, 176–189.

18 Y. Hovav, A. Feintuch and S. Vega, *J. Magn. Reson.*, 2012, **214**, 29–41.

19 A. Karabanov, A. van der Drift, I. Kuprov, L. J. Edwards and W. Köckenberger, *PCCP*, 2012, **14**, 2658–2668.

20 A. Karabanov, G. Kwiatkowski and W. Köckenberger, *Appl. Magn. Reson.*, 2012, **43**, 43–58.

21 D. Shimon, Y. Hovav, A. Feintuch, D. Goldfarb and S. Vega, *PCCP*, 2012, **14**, 5729–5743.

22 Y. Hovav, D. Shimon, I. Kaminker, A. Feintuch, D. Goldfarb and S. Vega, *PCCP*, 2015, **17**, 6053–6065.

23 A. Karabanov, D. Wiśniewski, I. Lesanovsky and W. Köckenberger, *Phys. Rev. Lett.*, 2015, **115**, 020404.

24 W. de Boer, *J. Low Temp. Phys.*, 1976, **22**, 185–212.

25 A. Abragam and M. Goldman, *Nuclear magnetism: order and disorder*, Clarendon Press, Oxford, 1982.

26 W. T. Wenckebach, *Essentials of dynamic nuclear polarisation*, Spindrift Publications, The Netherlands, 2016.

27 L. Lumata, A. K. Jindal, M. E. Merritt, C. R. Malloy, A. D. Sherry and Z. Kovasc, *J. Am. Chem. Soc.*, 2011, **133**, 8673–8680.

28 S. Jannin, A. Comment and J. van der Klink, *Appl. Magn. Reson.*, 2012, **43**, 59–68.

29 Y. Hovav, A. Feintuch and S. Vega, *PCCP*, 2013, **15**, 188–203.

30 A. D. Luca and A. Rosso, *Phys. Rev. Lett.*, 2015, **115**, 080401.

31 K.-N. Hu, V. S. Bajaj, M. Rosay and R. G. Griffin, *J. Chem. Phys.*, 2007, **126**, 44512–44519.

32 C. P. Pool and H. A. Farach, *Bull. Magn. Reson.*, 1980, **1**, 162–194.

33 O. Y. Rogozhnikova, V. G. Vasiliev, T. I. Troitskaya, D. V. Trukhin, T. V. Mikhalina, H. J. Halpern and V. M. Tormyshev, *Eur. J. Org. Chem.*, 2013, 3347–3355.

34 T. J. Reddy, T. Iwama, H. J. Halpern and V. H. Rawal, *J. Org. Chem.*, 2002, **67**, 4635–4639.

35 J. Granwehr, J. Leggett and W. Köckenberger, *J. Mag. Res.*, 2007, **187**, 266–276.

36 C. Reichardt, *Solvents and Solvent Effects in Organic Chemistry*, Wiley, Weinheim, 2004.